Research Paper

Skin friction directionality in monotonically- and cyclically-loaded bio-inspired piles in sand

Alejandro Martinez[1]* and Kyle O'Hara[2]

Abstract: Piles can be subjected to axial loading in opposite directions during their installation and service life. For instance, piles for offshore jacket structures and load testing reaction systems are subjected to compressive loading during installation and tensile or cyclic loading during service life. This creates a design dilemma: while a large skin friction can lead to refusal at shallower depths than required during driving, it also promotes a large pile axial capacity. This paper describes the load-transfer behavior of piles with surfaces inspired by the belly scales of snakes that mobilize a direction-dependent skin friction. The investigation presented herein consists of a series of twelve centrifuge pile load tests on bio-inspired and smooth reference piles in dense and loose deposits of Ottawa F65 sand. Test results indicate that greater skin friction forces are mobilized when the bio-inspired piles are displaced in the cranial direction (i.e. soil moving against asperities) relative to the caudal direction (i.e. soil moving along asperities). This is observed during pushing and driving installation, where greater skin friction forces were mobilized during installation by pushing in the cranial direction and driving in the cranial direction required more blows per meter. Similarly, the skin friction mobilized during pullout tests was between 82% and 198% greater in the cranial direction than in the caudal direction, and the skin friction mobilized during pullout by the bio-inspired pile in the cranial direction was between 560% to 845% greater than that mobilized by the reference untextured pile. During cyclic loading, degradation of the skin friction magnitude and pile secant stiffness was observed in both cranial and caudal directions; however, the mobilized magnitudes were generally greater in the cranial direction. Discussion is provided on the potential benefits that the bio-inspired surface texture could realize on the overall performance of axially-loaded piles.

Keywords: skin friction, shaft resistance, cyclic loading, centrifuge modeling, bio-inspiration

Introduction

Foundation elements can be subjected to axial loading in opposite directions during their installation and service life. Examples include piles and caissons supporting offshore jacket structures and piles for reaction systems for load tests. In both cases, foundations are loaded in axial compression during installation (e.g. driving, jacking) and in axial tension during their service life. This creates a design dilemma. On one hand, high skin friction loads are desirable to produce a large tensile capacity, but they can result in adverse conditions during installation (e.g. refusal, hard driving). On the other hand, small skin friction loads can improve installation conditions, but they can result in excessive settlements. Another example is piles in settling ground due to consolidation of clays or sand liquefaction, where the soil above the neutral plane (N.P.) generates down-drag loads while the soil below the N.P. provides upward skin friction capacity. Figure 1 presents schematics of situations where skin friction can develop in both upward and downward directions. Load transfer between the pile and the soil is a critical element for design and performance. The pile-soil interactions are accounted for in design methods for statically-loaded piles such as the β, Norlund, API, UWA, and ICP-05 methods as well as in t-z models (Lehane *et al.*, 2005; FHWA GEC 12). The soil-pile interactions are also accounted for in the design for down-drag loads (e.g. Fellenius, 1972; Boulanger and Brandenberg, 2004) and in the design calculation for the installation of caissons for offshore structures (e.g. Houlsby and Byrne, 2005).

Developing large or small skin friction loads for a given pile can bring benefits at different points during its lifetime. The interactions at the soil-pile interface during axial loading are typically independent of the load direction for vertical (i.e. non-tapered) piles; that is, the soil-pile interface friction angle is the same whether the pile is loaded in compression or

[1] Assistant Professor, University of California Davis, Davis, CA, USA

[2] Graduate Student Researcher, University of California Davis, Davis, CA, USA

* Corresponding author, email: amart@ucdavis.edu

Print ISSN: 1937-5247 Online ISSN: 1937-5255

Received 31 August 2020; received in revised form 13 March 2021; accepted 27 March 2021
https://doi.org/10.37308/DFIJnl.20200831.222

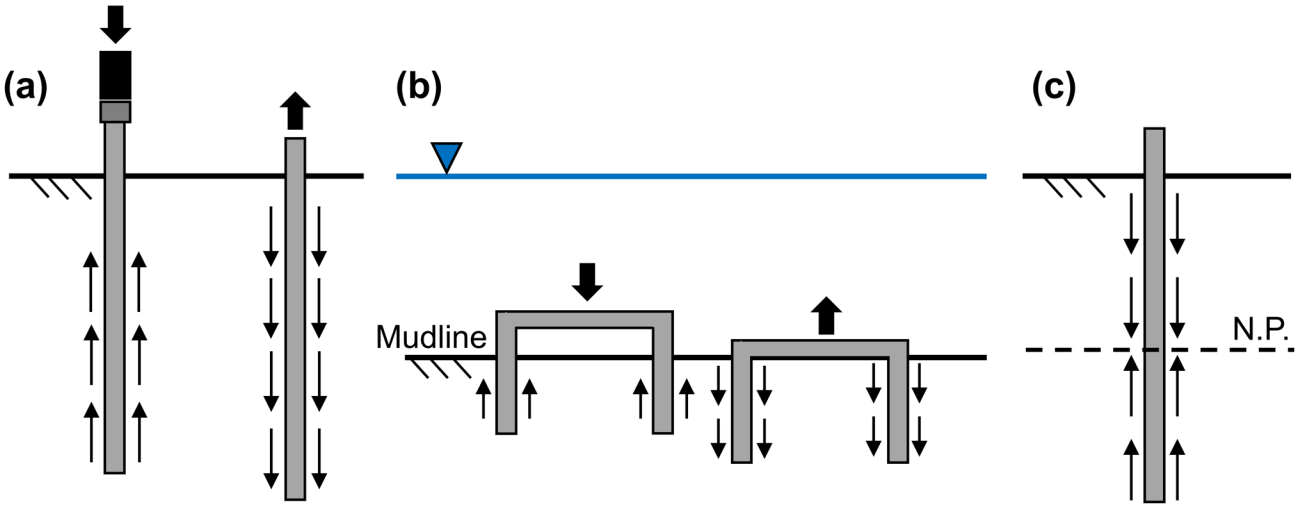

Figure 1. Examples of foundation elements loaded in opposite directions during their service life: (a) pile during driving and tensile loading, (b) offshore suction caisson during installation and tensile loading, and (c) pile in settling ground (note: arrows indicate soil skin friction forces, N.P. = Neutral Plane)

tension. However, the overall efficiency of piles and caissons loaded in tension and of piles in settling ground could be improved if their surface texture is designed to either maximize or minimize the transfer of load depending on the direction of loading. For piles and caissons, this could result in a greater skin friction capacity mobilized during tensile loading than during installation. For piles in settling ground, the downdrag loads above the N.P. could be reduced while the upward acting skin friction below the N.P. could be increased, potentially reducing the load transferred to the pile base and the resulting settlements.

A number of animals and plants have developed solutions, through the process of evolution, for transferring different amounts of frictional load in different directions. These solutions are present for example in snake belly scales (e.g. Marvi and Hu, 2012), cat tongues (e.g. Noel and Hu, 2018), and grass leaves (e.g. Kulic *et al.*, 2009). Two distinct mechanisms contribute to the difference in friction coefficients mobilized in different directions: (i) the asymmetric shape of the asperities and (ii) bending of the asperities that changes the interface contact area.

Bio-inspiration consists of leveraging successful natural solutions by adapting them to engineering problems. The field of bio-inspired geotechnics has received increasing attention during the last decade (Martinez *et al.*, 2021), resulting in advances in site characterization and sensor deployment (e.g. Huang and Tao, 2020; Martinez *et al.*, 2020; Chen *et al*. 2021; Borela et al. 2021), soil anchors (e.g. DeJong *et al.*, 2017; Burrall *et al.*, 2020), and load transfer at soil-structure interfaces (e.g. Martinez *et al.*, 2019). Particularly, Martinez *et al.* (2019) and O'Hara and Martinez (2020), Stutz and Martinez (2021) investigated the transfer of load between soils and surfaces inspired by snake belly scales. These studies showed a clear difference in the load transfer behavior at soil-structure interfaces when, relative to the bio-inspired surface, the soil is displaced along the scales (referred to as the "caudal" direction in biology) compared to when the soil is displaced against the scales (referred to as the "cranial" direction). Cranial shearing consistently results in greater interface peak and residual friction angles and dilation.

This study evaluates the directionally-dependent skin friction behavior of piles with snake skin-inspired surfaces and explores the implications and potential applications to deep foundations. A series of twelve centrifuge pile load tests were performed on four bio-inspired piles and a reference smooth pile at an acceleration of 40 times Earth's gravity on deposits of loose and dense sand. The piles were installed by either pseudo-static pushing or driving and then subjected to pullout tests. In addition, two of the tests involved cyclic loading after the pullout test. The results of the pile load tests shed light on differences in the load transfer response of the piles during installation and pullout loading considering the effect of the bio-inspired texture orientation relative to the direction of loading, installation method (i.e. pseudo-static pushed and driving), and sand density. Additional results from laboratory interface shear tests provide insight on the effect of asperity geometry and cyclic loading on the load transfer behavior of the bio-inspired surfaces and sandy soil.

Materials and Methods

Bio-inspired Piles

The surfaces used in this study were modeled after the belly scales of sixty preserved snake specimens on loan from the UC Berkeley Museum of Vertebrate Zoology. Each specimen was scanned using a white light scanner to produce a 3D image of its belly scales, as shown in Figure 2a for a western hognose snake, and a 2D profile was taken along the snake's longitudinal axis. Inspection of the sixty specimen profiles revealed that the scales can be grouped in three categories based on shape: concave up, concave down, and straight. Figure 2a shows an example of a straight-shaped profile, along with definitions for the asperity length (L) and asperity height (H). Model piles were manufactured with as-

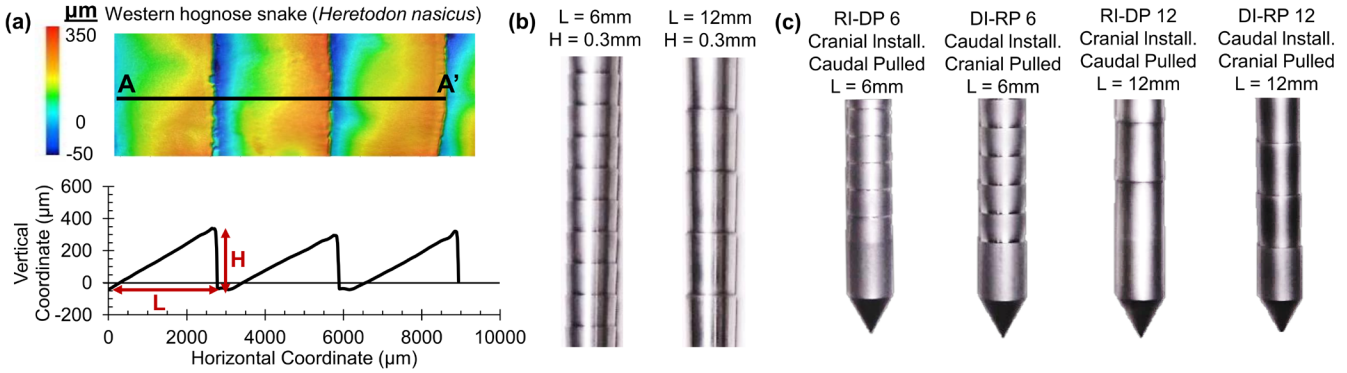

Figure 2. (a) 3D scan and profile along A-A' of western hognose snake belly scales, and (b) surface and (c) tip of bio-inspired piles for centrifuge pile load testing (L = asperity length, H = asperity height)

Table 1. Geometrical characteristics of bio-inspired piles

Pile	Installation Direction	Pullout Direction	Asperity Length (mm)
RI-DP 6	Cranial	Caudal	6
DI-RP 6	Caudal	Cranial	6
RI-DP 12	Cranial	Caudal	12
DI-RP 12	Caudal	Cranial	12

Note: R = Cranial, D = Caudal, I = Installation, P = Pullout

perity lengths of 6 and 12mm and a unique asperity height value of 0.3mm, as shown in Figure 2b. This selection was based on previous laboratory interface shear testing results by Martinez *et al.* (2019), who tested 20 different snake skin-inspired surfaces. Their results indicated that the surfaces with asperity lengths of 6 and 12mm and an asperity height value of 0.3mm (ratio of length to height of 40 and 20) consistently mobilized greater interface friction angles and induced greater soil shear strains in the cranial direction than in the caudal direction. The straight asperity shape as shown in Figure 2a was adopted for model piles because it facilitated the manufacturing process.

Four bio-inspired model piles were manufactured with brushed stainless steel, shown in Figures 2b and 2c. The pile texture was machined with a given orientation such that installation and subsequent pullout took place in either cranial or caudal shearing. For convenience, the piles are referred to throughout this paper according to the orientation of their texture and asperity length. The pile names and characteristics are listed in Table 1, where R is cranial, D is caudal, I is installation, P is pullout, and the number is the asperity length in mm. For instance, pile RI-DP 6 corresponds to the cranially installed – caudally pulled pile with an asperity length of 6mm.

Centrifuge Pile Load Testing

Centrifuge modeling has been routinely employed to investigate the behavior of geotechnical structures at field scales, such as deep and shallow foundations, tunnels, and slopes (e.g. Mason *et al.*, 2013; Loganathan *et al.*, 2000; Nova Roessig and Sitar, 2006). Particularly, the performance of piles under static and dynamic axial and lateral loads has been investigated by authors such as Nicola and Randolph (1999), Fioravante (2002), and Abdoun *et al.* (2003). By spinning a model in a geotechnical centrifuge, the gravity that the model experiences is increased due to the centrifugal acceleration. This allows matching the magnitude and distribution of the soil effective stresses relevant to the field application in a scaled model. The centrifuge scaling laws depend on the gravitational acceleration (N) that is applied to the model (Garnier *et al.*, 2007). It is customary in centrifuge modeling to refer to the full-scale structure being modeled as the "prototype" and to the actual small-scale model as the "model"; this convention is adopted throughout this paper. Scaling laws that are relevant to centrifuge modeling of piles are in Equations 1-4 in Table 2. More information regarding centrifuge scaling laws can be found in Kutter et al. (1992) and Garnier *et al*. (2007).

In this investigation, a series of pile load tests were performed at the UC Davis Center for Geotechnical Modeling (CGM) 9-m radius beam centrifuge. This centrifuge can subject a specimen of about 1550 kg of soil to a centrifugal acceleration equivalent to 75 times Earth's gravity. More information on the 9-m radius centrifuge at the CGM can be found in Boulanger et al. (2020). The acceleration applied to all the models was 40 times Earth's gravity, resulting in an N of 40. The model piles, shown in Figures 2b and 2c, have a diameter of 10mm and a length of 350mm in model scale, resulting in a diameter of 0.4m and a length of 14m in prototype scale. The pile tips were machined with a 60° apex angle cone to reduce the stresses during installation and the pile surfaces were machined with the textures shown in Figures 2b and 2c. The asperity lengths in model scale are 6 and 12mm for respective prototype scale L values of 0.24 and 0.48m, and the asperity height in model scale is 0.3mm for an H of 0.012m in prototype scale. A distance equivalent to two pile diameters behind the pile tip was left untextured to minimize the interactions between the tip and the surface texture. One additional untextured pile made from brushed stainless steel with an instrumented tip was used to provide results for comparison and is referred to herein as the "reference pile."

The piles were installed in-flight either by pseudo-static pushing with a hydraulic actuator or by driving with a hammer. A pseudo-static pushing rate of 10mm/s was selected

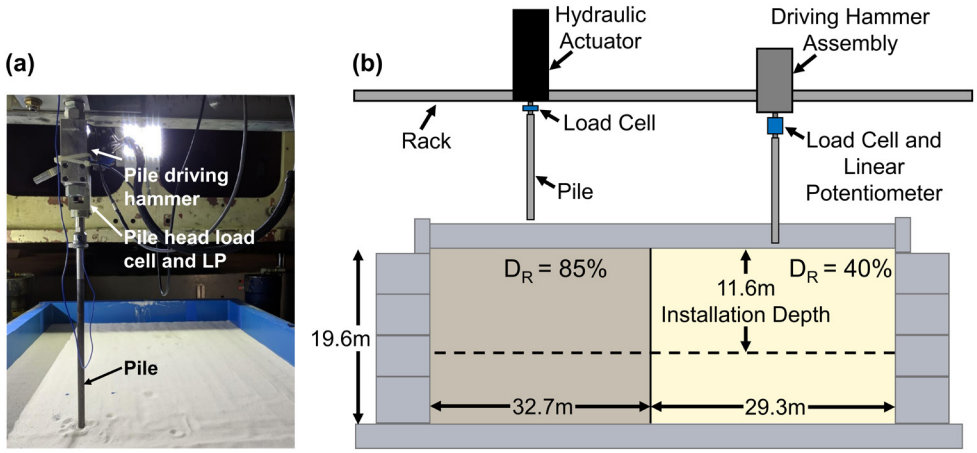

Figure 3. (a) Photograph of pile driving and pullout system, and (b) schematic of centrifuge model and loading system with prototype dimensions

based on previous results which indicate negligible inertial or strain-rate effects in dry sand at this pushing velocity (e.g. Darby et al. 2019). The driving hammer had a weight of 800N in prototype scale and it was allowed to free fall from a prototype height of 0.48m above the pile head (0.5N and 12mm, respectively, in model scale). A plastic cushion was placed on the pile head to protect it and to avoid strong high-frequency vibrations. The target installation depth of all piles was 11.6m, which was achieved for all the pushed piles. However, shallower depths between 6.75 and 10.4m were achieved during pile driving due to refusal. The forces and displacements during pushing installation and subsequent pullout and cyclic loading were measured with a load cell and linear potentiometer (LP) sensor installed at the pile head. Figure 3a shows a photograph of the driving hammer, pile head load cell and LP, and pile during driving and Figure 3b shows a schematic of the centrifuge model and pile load testing setup.

The pile load tests were performed in a deposit of dry Ottawa F65 sand. The deposit was prepared by air pluviation in lifts with a thickness of 75mm, for a total depth of 490mm (19.6m in prototype scale). The flow rate of the sand exiting the pluviator as well as the drop height were modified to achieve uniform deposits of different densities (Sturm *et al.*, 2018). The deposit was prepared in two halves: one half with dense sand (total unit weight (γ_t) = 16.8kN/m^3, void ratio (e) = 0.57, relative density (D_R) = 85%) and the other half with loose sand (γ_t = 15.4kN/m^3, e = 0.71, D_R = 40%), as shown in Figure 3b. Ottawa F65 is a poorly graded silica sand with a mean particle size (D_{50}) of 0.20mm, coefficient of uniformity (C_U) of 1.21, coefficient of curvature (C_C) of 1.00, minimum and maximum void ratios (e_{min} and e_{max}) of 0.52 and 0.83, respectively, and a direct shear residual friction angle (φ'_{res}) of 30° (Palumbo, 2018; Carey *et al.*, 2019). The particle size of the Ottawa F65 sand results in a ratio of the pile diameter to particle diameter of 50, which has been reported to result in negligible scale effects on the penetration resistance and shaft friction of penetrometers and piles by Bolton *et al.* (1999) and Fioravante (2002).

Centrifuge Pile Load Tests

A total of twelve pile load tests were performed as part of this study as follows: five on pushed piles in dense sand, three on pushed piles in loose sand, two on driven piles in dense sand, and two on driven piles in loose sand, as shown in Table 3. This testing program allowed examining the effects of the bio-inspired texture orientation (by comparing test pairs, e.g. #1 to #2, #3 to #4, #5 to #6, #9 to #10, and #11 to #12), asperity length (by comparing tests #1 to #3 and #2 to #4), sand density (by comparing tests #1 and #2 to #5 and #6), and installation method (by comparing tests #1, #2, #5, and #6 to #9-#12). In addition, the tests on the smooth, reference piles provide a baseline case for comparison against the bio-inspired piles in dense and loose sand deposits.

Following installation by pushing or driving, the piles were subjected to a 20mm pullout test. This displacement is equivalent to two pile diameters, which was selected to fully-mobilize the shaft resistances along the pile's length. In addition, two of the pushed piles in dense sand (Tests #1 and #2, Table 3) were subjected to cyclic loading with a displacement amplitude of 0.5mm. This was done to examine the degradation of skin friction with continuing cyclic loading. It should be recognized that the preceding pullout test likely caused some skin friction degradation. However, since the same testing sequence was employed in Tests #1 and #2, the results are likely affected in the same way. This allows for comparison of the results between these two tests.

A given pile's asymmetric surface results in skin friction mobilization in either the cranial or caudal direction depending on the direction of loading. For convenience, the results are referred to according to the direction of loading, where a given pile is installed and pulled in opposite directions. For instance, the RI-DP piles (Table 2) is installed in the cranial direction and pulled in the caudal direction while the DI-RP piles (Table 2) are installed in the caudal direction and pulled in the cranial direction.

The forces measured at the pile head indicate differences in the capacity mobilized during installation and subsequent

pullout. Figure 4 presents the prototype pile head force time history for the RI-DP 12 and DI-RP 12 piles in dense sand (Tests #1 and #2). The results highlight the difference in forces mobilized in the cranial and caudal directions. During installation, the RI-DP 12 pile generated greater forces as compared to the DI-RP 12 pile, with a prototype force value at an embedment depth of 11.6m of 7.9MN for the former and of 5.9MN for the latter. These pile head forces reflect the combination of the pile base and skin friction forces; however, only the skin friction is engaged during pullout loading. The pile head load after 20mm of pullout was -0.6MN for the RI-DP 12 pile and -1.8MN for the DI-RP 12 pile. These results show that the difference in pile head force between the RI-DP and DI-RP piles is controlled by the orientation of the texture, where loading in the cranial directions (whether during installation or pullout) mobilizes greater forces than loading in the caudal directions. The results of the cyclic tests are discussed in the "Pile Cyclic Loading" section of this paper.

Table 2. Centrifuge scaling laws

Scaling	Condition	Eq. #	Scaling	Condition	Eq. #
Length	$L_P = NL_M$	1	Depth	$Z_P = NZ_M$	2
Weight	$F_P = N^2F_M$	3	Soil Effective Stress	$\sigma'_{v,p} = \sigma'_{v,m}$	4

L = length; Z = depth; σ'_v = vertical effective stress; F = force; the subscripts $_P$ and $_M$ refer to the prototype and model scales.

Table 3. Details of centrifuge pile load tests

Test #	Pile	Asperity Length, *L* (mm)	Installation Method	Sand Relative Density, D_R (%)	Cyclic Loading
1	DI-RP 12	12	Pushed	85	Yes
2	RI-DP 12	12	Pushed	85	Yes
3	DI-RP 6	6	Pushed	85	No
4	RI-DP 6	6	Pushed	85	No
5	DI-RP 12	12	Pushed	40	No
6	RI-DP 12	12	Pushed	40	No
7	Reference	-	Pushed	85	No
8	Reference	-	Pushed	40	No
9	DI-RP 12	12	Driven	85	No
10	RI-DP 12	12	Driven	85	No
11	DI-RP 12	12	Driven	40	No
12	RI-DP 12	12	Driven	40	No

Pile Installation

Eight piles were installed by pseudo-static pushing and four piles were installed by driving (Table 3). The reference pile had an instrumented tip that measured the base resistance load during pushing installation, as presented in Figure 5a. At a depth of 11.6m, the prototype base loads were 3.62 and 0.77MN in the dense and loose sand, respectively, which result in unit base resistances of 28.8 and 6.1MPa. The skin friction load at any given depth (SFL_{Zi}) during installation was computed as follows:

$$SFL_{Zi} = THL_{Zi} - BL_{Zi} \quad (5)$$

where THL = total pile head load, BL = base load, and the subscript $_{Zi}$ denotes any given depth. The computed skin friction loads for the reference pile are shown in Figures 5b and 5c for the dense and loose sand deposits, respectively. As expected, the skin friction during installation was greater in the dense sand than in the loose sand.

The bio-inspired pile texture orientation had an important effect on the magnitude of skin friction load mobilized during installation. Since the bio-inspired piles were not in-

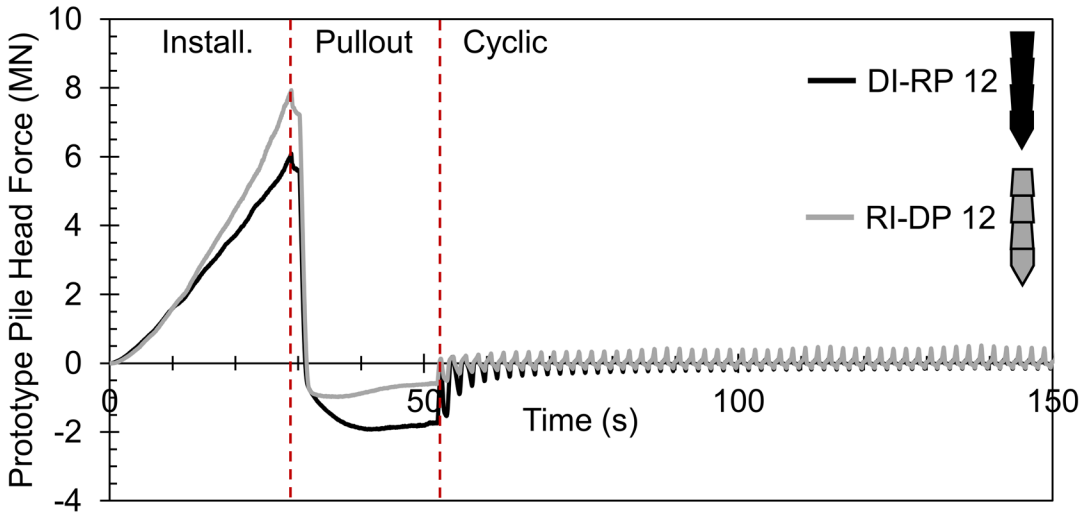

Figure 4. Time series of prototype pile head force measurements during in dense sand for piles DI-RP 12 and RI-DP 12 (Tests #1 and #2)

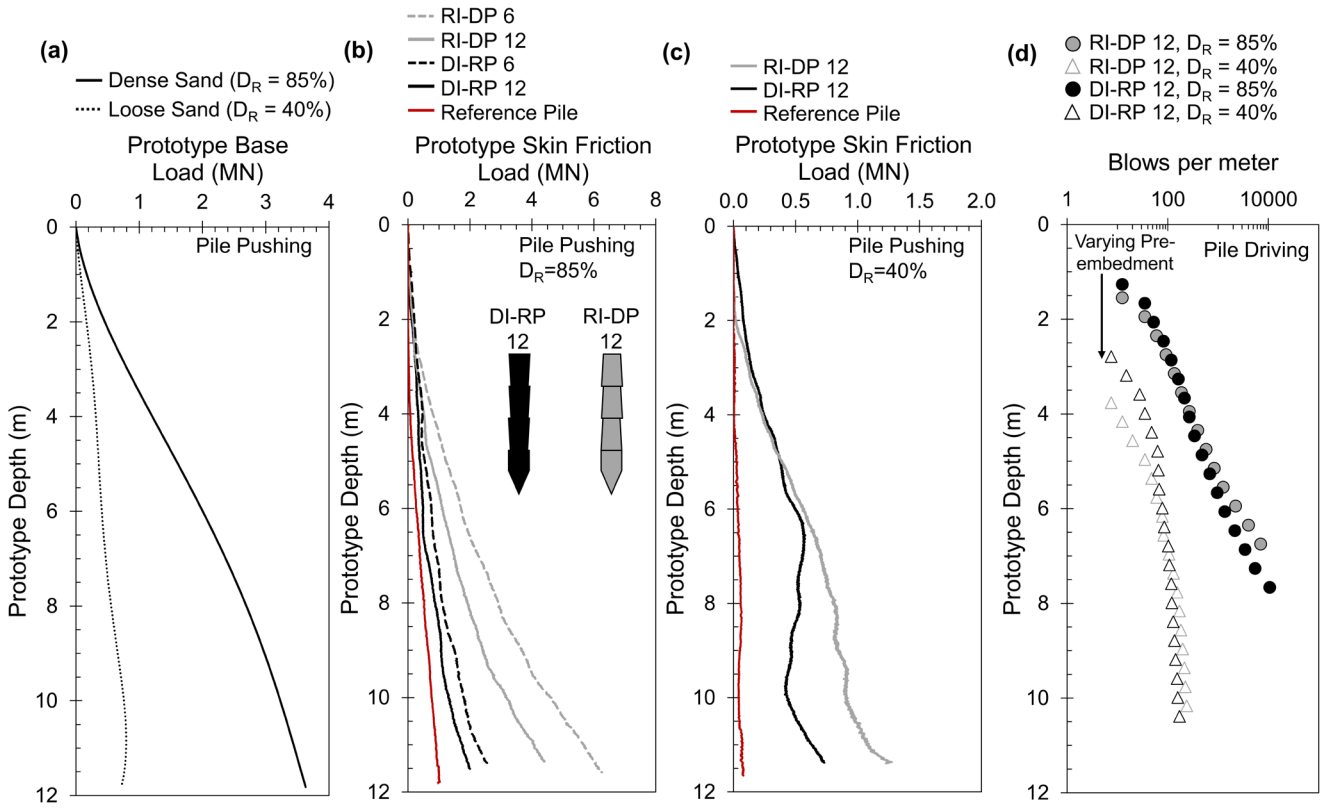

Figure 5. (a) Base load during pile pushing in dense and loose sand, (b) skin friction load during pile pushing in dense sand (Tests #1-#4 and #7), (c) skin friction during pile pushing in loose sand (Tests #5-#6 and #8), and (d) blows per meter during pile driving in dense and loose sand (Tests#9-#12) (note the different x-axis ranges in (a), (b), and (c))

strumented to measure the base load, their base loads in dense and loose sand were assumed to be equal to the base load measured by the reference pile in the sand with corresponding D_R. Subsequently, Equation 5 was used to compute the skin friction load during installation. Figure 5b shows the results for tests on piles with asperity length, L, of 6 and 12mm in dense sand while Figure 5c shows the results for tests on piles with an L of 12mm in loose sand. The results show that significantly greater skin friction loads are mobilized during cranial installation than during caudal installation in both dense and loose sand deposits, particularly at depths from 6.0 to 11.6m. For instance, the RI-DP 12 pile in dense sand mobilized a skin friction load of 4.4MN at a depth of 11.6m, whereas the corresponding value for the DI-RP 12 pile is 2.0MN. The results presented in Figure 5b show the effect of the asperity length on the magnitude of mobilized skin friction loads, where the piles with the shorter asperities mobilized greater loads during both caudal and cranial installation than the piles with an L of 12 mm.

The difference in skin friction mobilized in the cranial and caudal directions is also appreciable during driving. Figure 5d presents results in terms of blows per meter. It should be noted that the piles were pre-embedded in-flight at varying depths between 1.25 and 3.75m before the autonomous pile driving system could be engaged. The results show that the RI-DP 12 (cranially installed) piles required more blows per meter at depths greater than 4m in dense sand and 6m in loose sand. The greater blows per meter at shallower depths for the caudally installed piles are believed to reflect the different pre-embedment depths which were smaller for the DI-RP 12 (caudally installed) piles in both dense and loose sand. Both piles reached a refusal condition in dense sand; this took place at a depth of 6.8m with over 7,000 blows per meter for the RI-DP 12 pile and at a depth of 7.4m with about 5,400 blows per meter for the DI-RP 12 pile.

Pile Pullout Behavior

Pullout tests were performed following installation to establish the skin friction capacity of the model piles. The average mobilized unit skin friction, τ_{avg}, was computed during pullout as the ratio of the total force measured at the pile head to the shaft's embedded surface area, whereas the average vertical effective stress, $\sigma'_{v,avg}$, was calculated at the mid-pile embedment depth. The results are analyzed using the effective stress approach, as follows:

$$\tau_{avg} = \sigma'_{r,avg} tan(\delta') \quad (6)$$

where $\sigma'_{r,avg}$ = average radial effective stress acting on the pile surface and δ' = effective interface friction angle. Since $\sigma'_{r,avg}$ is typically unknown, it is often expressed in terms of the lateral earth pressure coefficient K_{avg}, as follows:

$$\sigma'_{r,avg} = \sigma'_{v,avg} K_{avg} \quad (7)$$

In practice, it is common to estimate τ_{avg} based on a back-calculated β coefficient (e.g. Chen and Kulhawy, 1994; Fioravante *et al.*, 1999) from field tests, as follows:

$$\tau_{avg} = K_{avg}\,\sigma'_{v,avg}\tan(\delta') = \beta\sigma'_{v,avg} \quad (8)$$

where β represents the product of K_{avg} and $\tan(\delta')$. Results are presented in this analysis in terms of the stress ratio, $\tau_{avg} / \sigma'_{v,avg}$. This normalizes the influence of varying embedment depth on τ_{avg}. In addition, the $\tau_{avg} / \sigma'_{v,avg}$ parameter is equivalent to the β coefficient in Equation 8.

The pullout curves for all the pushed piles indicate a clear effect of the texture orientation, where pulling in the cranial direction resulted in greater shear stresses and associated stress ratios. Figure 6a shows the pullout curves for the pushed piles in dense sand, showing that the cranially pulled piles consistently mobilized greater stress ratios than the caudally pulled piles. The difference in mobilized stress ratios is large, with residual stress ratio values of 1.76 and 1.49 for the DI-RP 6 and DI-RP 12 piles, respectively, and residual stress ratio values of 0.63 and 0.47 for the RI-DP 6 and RI-DP 12 piles. As shown, the piles with smaller L mobilized greater skin friction, in agreement with laboratory interface shear results presented by Martinez *et al.* (2019). The results of the load tests in loose sand also show that a greater skin friction is mobilized during cranial pullout (pile DI-RP 12) than during caudal pullout (pile RI-DP 12), as shown in Figure 6b. The reference piles mobilized the smallest skin friction in both dense and loose sand, likely due to their smoother surface texture. This agrees with results from pile load tests and laboratory studies indicating that the friction angle and dilation of soil-pile interfaces increases as the surface roughness of the pile is increased (Jardine *et al.*, 1992; Tehrani *et al.*, 2016; Martinez and Frost, 2017).

Differences were also observed in the secant pile stiffness, k, calculated as the ratio of the unit skin friction to the shear displacement. Figure 6c presents k values calculated at a shear displacement of 0.5mm, showing that the pile stiffness was significantly greater for the piles in dense sand than for the piles in loose sand. In addition, the pullout curves in the caudal direction (RI-DP 12 pile) have greater k values than the pullout curves in the cranial direction (DI-RP 12 pile). The caudal k is 17% and 27% greater than the cranial k in dense and loose sand, respectively. These results reflect the failure mechanism at the soil-pile interface, where a sliding failure mechanism at the interface is characterized by a stiffer and more brittle load transfer response (Martinez *et al.*, 2015). For the case of the bio-inspired surfaces, Martinez *et al.* (2019) showed that caudal shearing results in a greater amount of sliding at the interface than cranial shearing, which agrees with the greater k observed during the caudal pullout tests in this study.

The driven piles mobilized greater stress ratios in both dense and loose sand than the pushed piles. Figures 7a and 7b provide a comparison for the DI-RP 12 and RI-DP 12 piles in dense and loose sand. As shown, the driven piles exhibited a peak stress ratio followed by strain softening, especially in dense sand. The difference between driven and pulled piles is especially clear for the DI-RP 12 piles. This difference likely reflects the different state of stresses mobilized around the piles during installation, where installing in the caudal direction may result in greater stresses acting on the pile surface in a similar way as has been observed for tapered piles (e.g. Wei and El Naggar, 1998). Secant pile stiffness values were calculated over the initial 0.5mm of shear displacement as shown in Figure 7c. The results indicate the k of the cranial pullout tests (DI-RP 12 pile) was greater, possibly reflecting the greater normal effective stress acting on the pile surface at the initial stages of pullout testing.

The differences in skin friction can be analyzed using Equation 6. The two parameters that determine the τ_{avg} magnitude are $\sigma'_{r,avg}$ and δ'. Martinez *et al.* (2019) made δ' measurements in Ottawa F65 sand in the cranial and caudal directions. The authors reported cranial δ' values of 40.4° and 35.8° for surfaces with an L of 6 and 12mm, respectively, and caudal values of 35.0° and 30.9° for surfaces with an L of

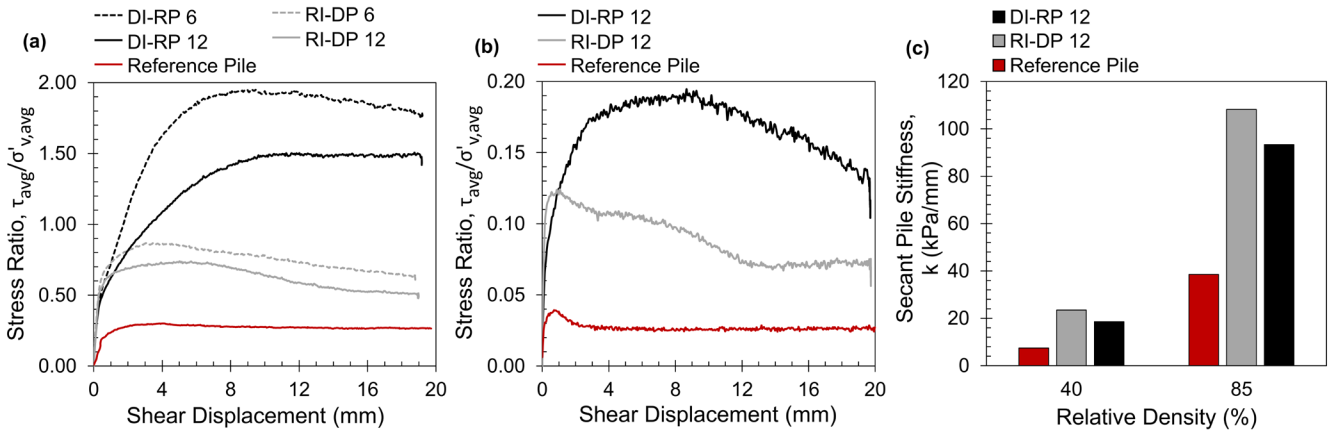

Figure 6. Pullout test data on pushed piles in (a) dense (D_R = 85%, Tests #1-#4 and #7), and (b) loose sand (D_R = 40%, Tests #5-#6 and #8) (note different y-axis ranges), and (c) secant pile stiffness at 0.5mm of shear displacement

6 and 12mm, respectively. For the same $\sigma'_{r,avg}$, the differences in δ' in the cranial and caudal directions result in τ_{avg} differences of 21%. However, the stress ratios mobilized during cranial pullout were significantly greater than those mobilized during caudal pullout. For instance, the residual cranial stress ratio for pushed piles was an average of 128% and 82% greater than the caudal stress ratio in dense and loose sand, respectively, and 96% and 198% greater for the driven piles in dense and loose sand, respectively.

The large differences in τ_{avg} can be better explained by differences in the radial effective stress acting on the pile surface. The magnitude of $\sigma'_{r,avg}$ is influenced by the installation method and sand relative density (e.g. Salgado, 2008) as well as by the surrounding sand mass' stiffness and volumetric dilatancy of the soil in contact with the pile (Lehane *et al.*, 1993; White and Lehane, 2004). The evolution of $\sigma'_{r,avg}$ during pullout loading can be expressed in terms of the lateral earth pressure coefficient according to Equations 7.

Average lateral earth pressure values at the residual and peak conditions were calculated for the load tests on piles with an L of 12mm, as shown in Figures 8a and 8c. The results for the pushed piles indicate that their residual and peak K_{avg} from cranial pullout tests were greater than those from caudal pullout tests. Namely, the residual and peak K_{avg} val-

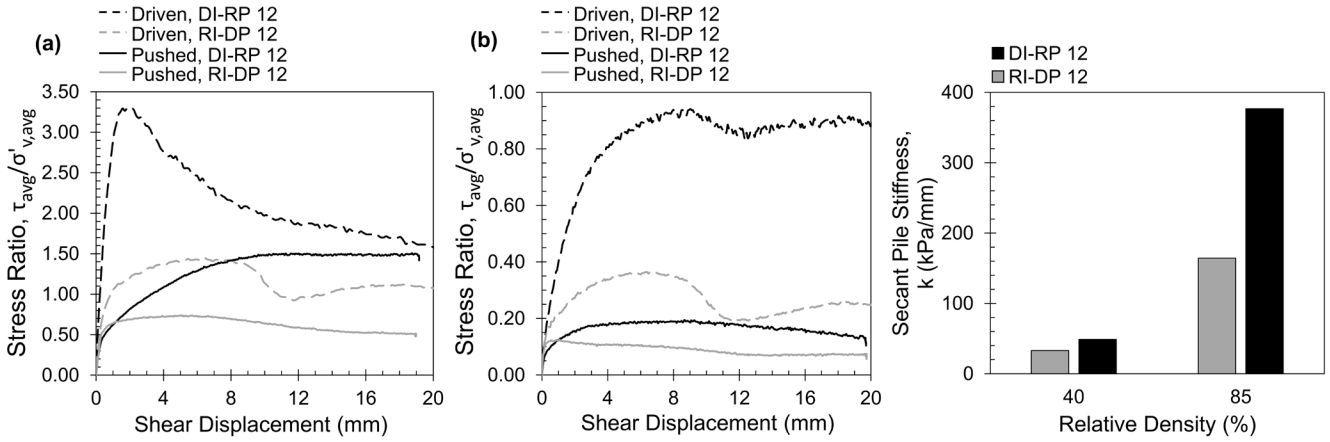

Figure 7. Comparison of pullout tests on driven and pushed piles with an L of 12mm in (a) dense (D_R = 85%, Tests #1-#2 and #9-#10) and (b) loose sand (D_R = 40%, Tests #5-#6 and #11-#12) (note different y-axis ranges), and (c) secant pile stiffness for driven piles at 0.5mm of displacement

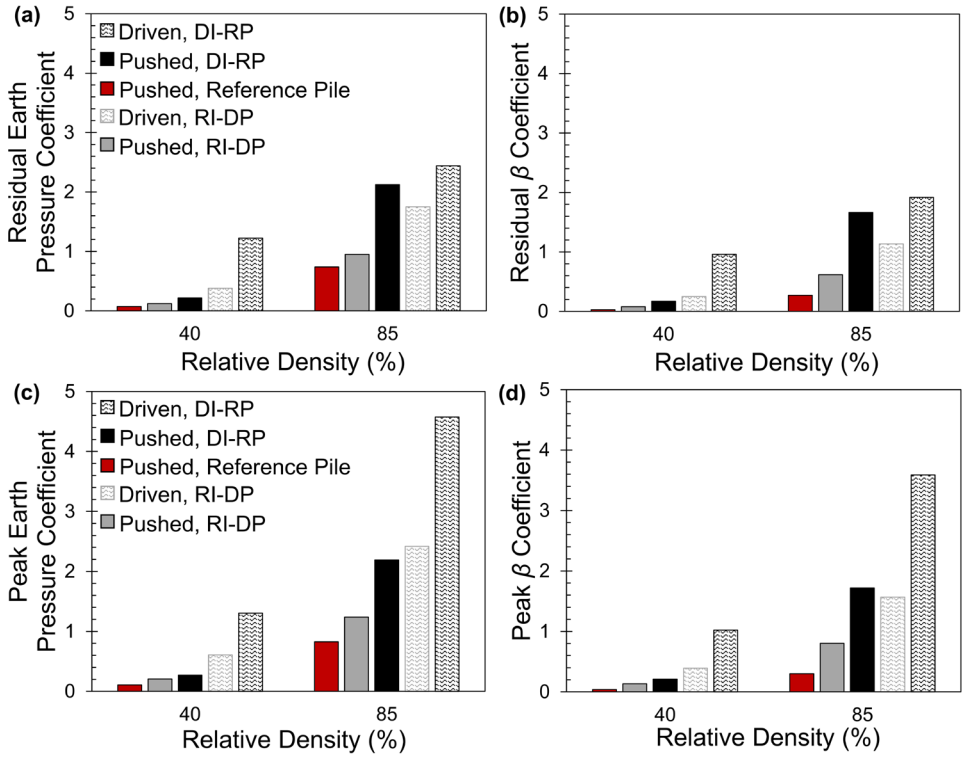

Figure 8. Back-calculated lateral earth pressure, K_{avg}, and β coefficients from pullout tests on piles with an L of 12 mm at (a) and (b) residual and (c) and (d) peak conditions

ues for the pushed DI-RP 12 pile were 2.14 and 2.19 in dense sand and 0.21 and 0.27 in loose sand. In contrast, the RI-DP 12 pile yielded residual and peak K_{avg} values of 0.95 and 1.24 in dense sand and 0.12 and 0.21 in loose sand. The K_{avg} values for the smoother reference piles were smaller, with a maximum value of 0.83 in dense sand and a minimum value of 0.08 in loose sand. These magnitudes and trends are in agreement with values from calibration chamber pile load tests reported by Tehrani *et al.* (2016), who obtained K_{avg} values that ranged from 0.51 to 3.25 and increased with sand D_R and pile surface roughness. The K_{avg} values were greater for the driven piles, with residual and peak values in the dense sand as high as 2.44 and 4.58 for the DI-RP 12 pile and as high as 1.75 and 2.42 for the RI-DP 12 pile.

The pullout test results can be analyzed in terms of the β coefficient, as shown in Figures 8b and 8d. The results show similar trends as those described for the K_{avg} parameter, with β coefficients that are greater during cranial pullout than caudal pullout, are greater for the driven piles than pushed piles, and increase as D_R is increased. The reported β values for the pushed piles are in general agreement with those reported by Fiviorante (2002) from centrifuge pile load tests, which increased with pile surface roughness and sand D_R and can be as high as 3.6.

Pile Cyclic Loading

Cyclic loading during pile installation and service life can result in degradation of the unit skin friction and pile stiffness (e.g. White and Lehane, 2004; Tsuha *et al.*, 2012). Displacement-controlled cyclic load tests with a double amplitude of 0.50mm were performed on the DI-RP 12 and RI-DP 12 piles in dense sand (Tests #1 and #2) to evaluate the cyclic behavior of the bio-inspired piles. The results revealed that the orientation of the bio-inspired texture influenced the degradation of skin friction and pile secant stiffness. Figures 9a and 9d present the results for the DI-RP 12 and RI-DP 12 piles, respectively, in terms of stress ratio (τ_{avg} / $\sigma'_{v,avg}$) versus shear displacement, while Figures 9b and 9e present the corresponding unit skin friction magnitudes at the end of each cycle in the tension and compression directions. The DI-RP 12 pile mobilized significantly greater unit skin friction in the cranial first direction than in the caudal second direction (Figure 9b). The cranial τ_{avg} value for the first cycle was 170 kPa, which rapidly degraded and reached a value of about 22 kPa after 25 cycles. In contrast, the caudal τ_{avg} increased slightly from an initial value of 20kPa to a value of about 22kPa after 25 cycles. The RI-DP 12 pile mobilized a greater τ_{avg} in the caudal first direction for the first three cycles. However, the caudal τ_{avg} rapidly degraded to about 16kPa while the cranial second τ_{avg} slowly increased to about 44kPa, possibly due to increased interlocking between the soil and the asperities. The secant pile stiffness at the end of each cycle was computed as the ratio of the unit skin friction to the shear displacement. The results indicate a similar trend as described for τ_{avg}, where k was significantly greater in the cranial direction for the DI-RP 12 pile, and the cranial k increased

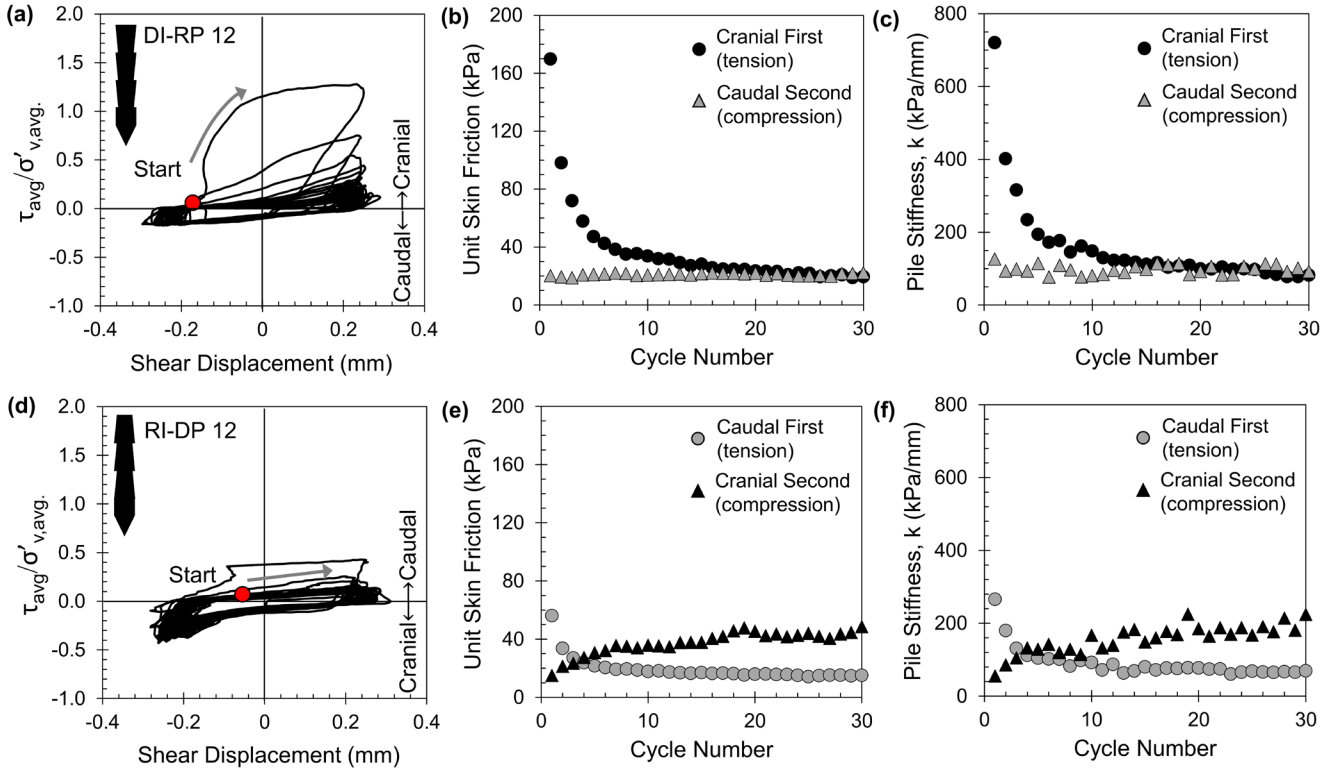

Figure 9. Cyclic pile load tests in dense sand with a cyclic displacement amplitude (δ_{cyc}) of 0.5mm: (a) stress ratio – shear displacement, (b) unit skin friction, and (c) pile stiffness for pile DI-RP 12 (Test #1) and (d) stress ratio – shear displacement, (e) unit skin friction, and (f) pile stiffness for pile RI-DP 12 (Test #2)

to a greater value than that in the caudal direction after three cycles for the RI-DP pile.

Discussion

Effect of Asperity Geometry

The results from the pile load tests indicate that the orientation of the bio-inspired texture has an important influence on the load transfer behavior at the soil-pile interface. Furthermore, the skin friction measured during installation and pullout testing is also influenced by the geometry of the asperities. As shown in Figures 5 and 6, the piles with a shorter asperity length consistently mobilized greater skin friction loads. This is likely because a smaller L results in a greater number of asperities per unit length of pile. Martinez *et al.* (2019) performed a laboratory interface shear tests on snake skin-inspired surfaces with varying asperity L and H. The authors used a shear box-type interface shear device and used constant normal load boundary conditions. The authors reported an increase in the interface friction angle as L was decreased and H was increased. The authors showed that the relationship between the peak and residual interface friction angle and the asperity geometry can be uniquely described with the L / H ratio, as shown in Figures 10a and 10b, which has been verified for loose and dense sub-rounded and sub-angular sands (Stutz and Martinez 2021). The relationship between δ' and the asperity geometry by way of the L / H parameter may be advantageous for design purposes, as it may allow engineers to design the pile surface texture to promote a specific load transfer behavior. For instance, a pile could be designed with different textured sections along its length, selecting a small L / H for sections where high skin friction capacity is beneficial and a large L / H where a smaller skin friction is desired.

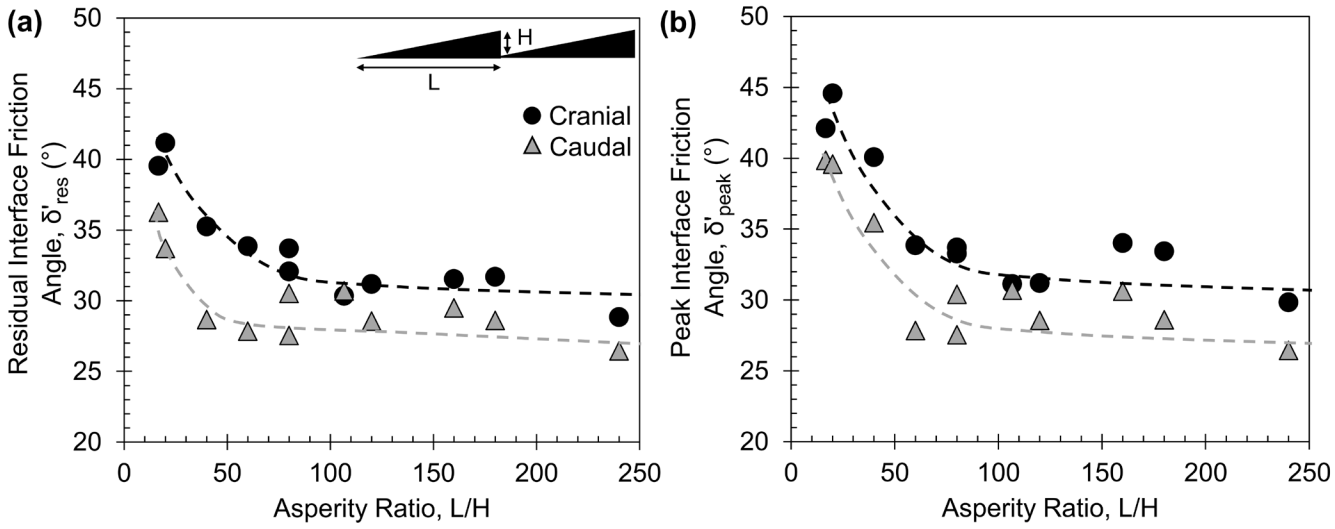

Figure 10. Influence of asperity geometry ratio on the (a) residual and (b) peak interface friction angle measured in constant normal load interface shear tests (D_R = 85%, normal effective stress = 75kPa) (data from Martinez *et al.*, 2019)

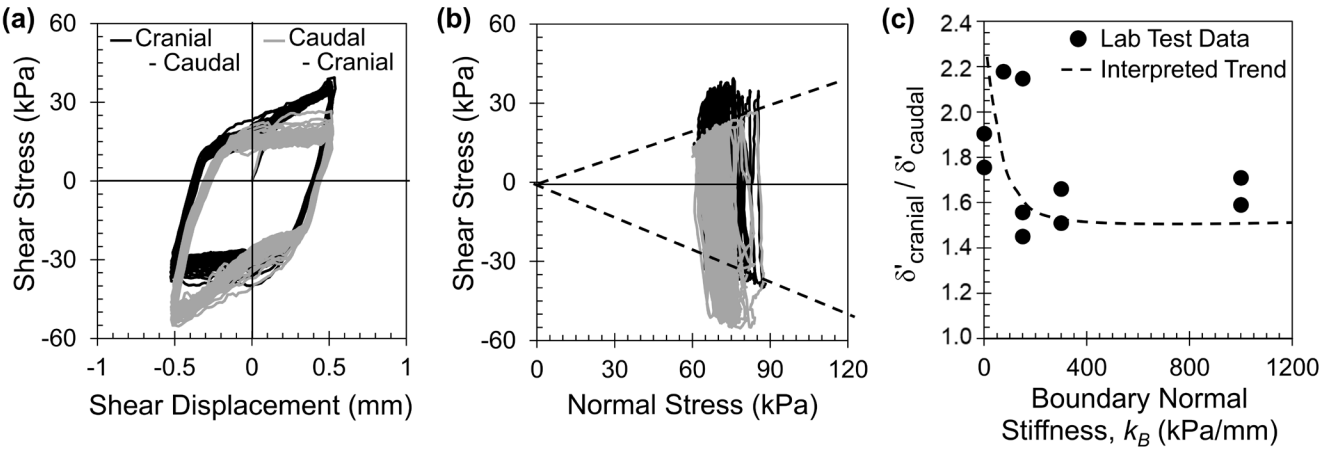

Figure 11. Displacement-controlled cyclic interface shear tests on dense sand. (a) Shear stress – shear displacement and (b) stress paths from tests (initial stress = 80kPa and k_B = 150kPa/mm; dashed line indicates the failure envelopes in the caudal direction), and (c) ratios of mobilized interface friction angles as a function of boundary stiffness (D_R = 85%, initial normal stress = 80kPa and k_B = 150kPa/mm; dashed line indicates the failure envelopes in the caudal direction)

Cyclic Skin Friction Degradation and Failure

The orientation of the asymmetric asperities can be used to create biases in the load transfer behavior. For instance, Figures 5, 6, and 7 show that cranial shearing results in greater skin friction loads mobilized in either compressive or tensile loading. The results shown in Figure 9 indicate differences in the mobilization and degradation of skin friction and stiffness during cyclic loading.

A bias in the skin friction behavior can be used to benefit specific engineering applications. This was further explored in regard to cyclic skin friction behavior through constant normal stiffness interface shear tests, as described by Boulon and Foray (1986) and Airey *et al.* (1992), while O'Hara and Martinez (2020) provide a description of the experimental setup used for this investigation. These tests allow the normal stress acting on the soil-structure interface to change during shearing according to the soil's dilatancy and the imposed boundary stiffness k_B, thus providing a feasible method to model the load transfer at a pile shaft (Boulon and Foray, 1986; Airey *et al.,* 1992). Cyclic tests were performed in the cranial first (positive shear stresses) and caudal second (negative shear stresses) sequence and *vice versa*. Displacement-controlled tests were performed to evaluate the degradation of skin friction capacity while load-controlled tests were performed to observe the accumulation of shear deformations. Figures 11a and 11b present the results of a displacement-controlled test on dense sand (D_R = 85%) with a cyclic amplitude of 1.0mm and a boundary stiffness of 150kPa/mm, which show that shearing in the cranial direction mobilized greater shear stresses in both cranial-caudal and caudal-cranial tests, where the dashed lines in Figure 11b represent the failure envelopes in the caudal direction. Figure 11c shows a summary of the interface friction angles mobilized in caudal-first tests performed with varying boundary stiffness. As shown by the $\delta'_{cranial} / \delta'_{caudal}$ ratios, shearing in the cranial direction consistently mobilized greater interface friction angles, with the difference decreasing as the boundary stiffness is increased.

Load-controlled tests were performed on dense sand specimens (D_R = 85%) with cyclic amplitudes, τ_{cyc}, of 21 and 25kPa in the caudal-cranial or cranial-caudal sequences. The results indicate that failure by pullout consistently occurred in the caudal direction, as shown in Figures 12a and 12b. Failure occurred on the caudal direction once the normal effective stresses reduced to a level that prevented the mobilization of the prescribed τ_{cyc} magnitude, as shown by the stress

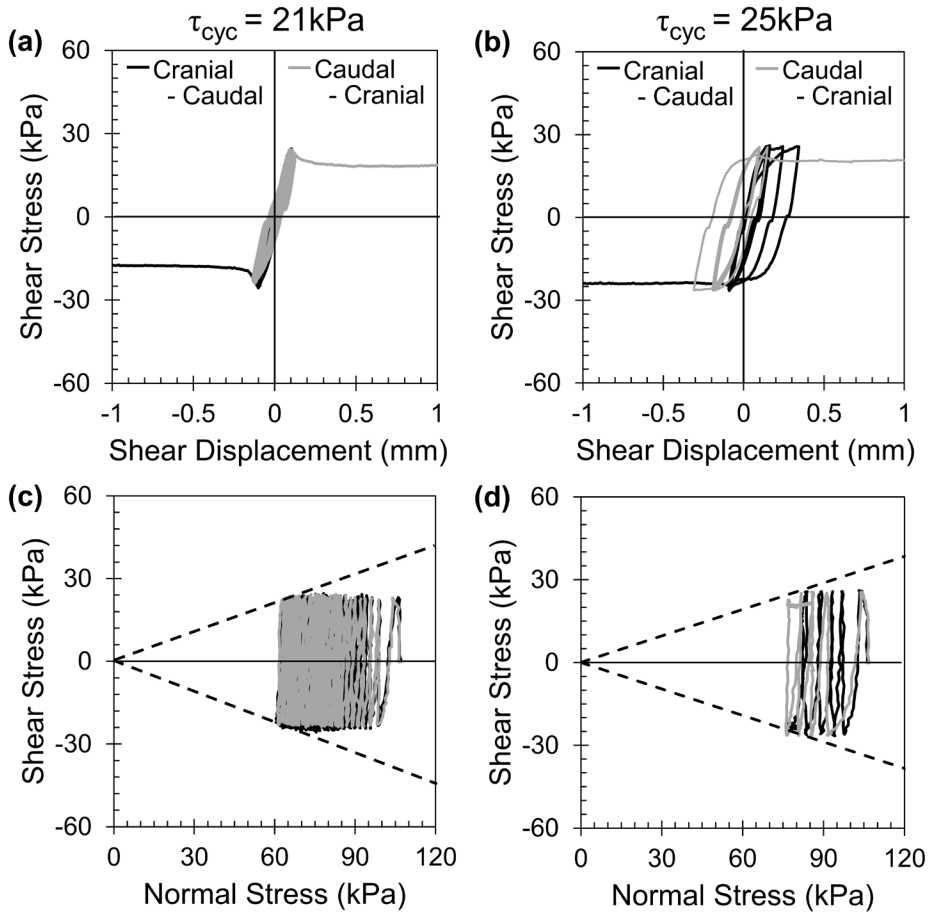

Figure 12. Load-controlled cyclic interface shear tests on dense sand, where (a) and (c) have a cyclic amplitude of 21kPa and (b) and (d) have a cyclic amplitude of 25kPa (D_R = 85%, initial normal stress = 108kPa, kB = 300kPa/mm; dashed line indicates the failure envelopes in the caudal direction)

paths in Figures 12c and 12d. These results show that the orientation of the asperities can be used to control the direction of pullout failure. This could be useful for cyclically-loaded foundations such as those supporting offshore jacket structures which can lose serviceability due to excessive pullout deformations. Piles or caissons configured in the caudal installation – cranial pullout asperity orientation could create a bias to reduce pullout deformations while engagement of the pile tip could prevent significant settlements.

Implications in Practice

The results presented in this paper highlight some of the benefits that could be realized by the bio-inspired piles. The load tests performed in this study highlight the dependence of the skin friction magnitude on the direction of loading relative to the orientation of the bio-inspired surface texture, where cranial shearing consistently mobilized greater skin friction loads than caudal shearing, and the smoother reference pile mobilized the smallest skin friction. The results of this investigation are summarized in terms of ratios of parameters measured in the cranial direction to those in the caudal direction and to those measured for the reference pile (Table 4) to give insight into the differences in skin friction. The cranial to caudal ratios are as high as 2.98 for the pullout capacity of driven piles and as low as 1.54 for the number of blows per meter during driving installation, highlighting the bias in skin friction load transfer that can be achieved. The cranial to reference pile ratios have values as high as 16.36 for pushing skin friction in loose sand and as low as 3.86 for the pushing skin friction in dense sand, indicating that the skin friction capacity in the cranial direction was significantly larger than that mobilized by the reference pile.

Several aspects need to be addressed before the new bio-inspired surfaces are adopted by industry. First, the distribution of load transfer along the pile length must be better understood. This could be addressed through tests with instrumented piles which would shed light on the local load transfer mechanisms. Second, field load tests on full-scale prototype piles should be performed to verify the trends reported in this investigation. Such tests would also enable the development of t-z relationships which would aid in design calculations. Finally, manufacturing procedures must be developed to economically produce piles with bio-inspired surfaces and to allow for their installation with existing construction equipment.

Conclusions

Results from centrifuge load tests performed on piles with surface texture inspired by snake belly scales in deposits of dense and loose dry sand show that the skin friction capacity and overall load transfer behavior is dependent on the direction of loading relative to the orientation of the asymmetric asperities. The main experimental observations of this study are as follows:

- Installation: Greater skin friction forces were mobilized during installation by pushing in the cranial direction (i.e. against the asperities) than in the caudal direction (i.e. along the asperities) in both dense and loose sand. This was also evident during pile driving, where driving in the cranial direction required more blows per meter, especially at greater depths.
- Monotonic loading: The difference in skin friction was also observed in the pullout tests, where pulling in the cranial direction mobilized skin friction that was between 82 and 198% greater than in the caudal direction. Back-calculated lateral earth pressure coefficients indicate that the radial effective stresses around the piles are greater during cranial loading.
- Cyclic loading: Degradation of the skin friction magnitude and the secant pile stiffness was observed during cyclic loading. However, the skin friction and stiffness mobilized in the cranial direction were generally greater than those mobilized in the caudal direction.

A unique aspect of the behavior of the bio-inspired piles is that the skin friction magnitude is distinctively different during compressive and tensile loading. This directionality in load transfer can be beneficial to develop new foundation types that, for instance, mobilize smaller skin friction resistance during installation than during subsequent tensile loading. The results from additional cyclic interface shear tests indicate that pullout failure consistently takes place in the caudal direction. This can provide opportunities to mitigate loss of serviceability of offshore structures due to progressive pullout if the texture is oriented such that tensile loading induces cranial shearing.

Table 4. Summary of average cranial to caudal and cranial to reference steel ratios from centrifuge pile load tests

	Cranial to Caudal				Cranial to Reference Steel	
Sand Density	**Pushing Skin Friction (MN/MN)[a]**	**Blows per m[b]**	**Pullout Capacity (Pushed Pile) (MN/MN)[c]**	**Pullout Capacity (Driven Pile) (MN/MN)[c]**	**Pushing Skin Friction[a] (MN/MN)**	**Pullout Capacity (Pushed Pile) (MN/MN)[c]**
Dense	1.68	2.67	2.28	1.96	3.86	5.60
Loose	1.56	1.54	1.82	2.98	16.32	8.45

[a]From of 5 to 11 mm, [b]From penetration depths of 3 to 6.3 m,[C]at the residual stage

Acknowledgments

The authors would like to acknowledge the contributions of Sumeet Sinha, Sophia Palumbo, Lin Huang, Jason DeJong, Katerina Ziotopoulou, and Daniel Wilson. This material is based upon work supported by the Engineering Research Center Program of the National Science Foundation under NSF Cooperative Agreement No. EEC-1449501. The UC Davis Center for Geotechnical Modeling is supported under the grant CMMI-1520581. Any opinions, findings, and conclusions or recommendations expressed in this material are those of the author(s) and do not necessarily reflect those of the National Science Foundation.

References

Abdoun, T., Dobry, R., O'rourke, T. D., & Goh, S. H. (2003). Pile response to lateral spreads: centrifuge modeling. *Journal of Geotechnical and Geoenvironmental Engineering*, 129(10), 869-878. doi:10.1061/(ASCE)1090-0241(2003)129:10(869)

Airey, D. W., Al-Douri, R. H., & Poulos, H. G. (1992). Estimation of pile friction degradation from shearbox tests. *Geotechnical Testing Journal*, 15(4), 388-392. doi:10.1520/GTJ10253J

Bolton, M. D., Gui, M. W., Garnier, J., Corte, J. F., Bagge, G., Laue, J., and Renzi, R. (1999). Centrifuge cone penetration tests in sand. *Géotechnique*, 49(4), 543-552. doi:10.1680/geot.1999.49.4.543

Borela, R., Frost, J.D., Viggiani, G., and Anselmucci, F. (2021). Earthworm-inspired robotic locomotion in sand: an experimental study with X-ray tomography. *Géotechnique* letters, 11(1), 66-73. doi:10.1680/jgele.20.00085

Boulanger, R. W., & Brandenberg, S. J. (2004). Neutral plane solution for liquefaction-induced down-drag on vertical piles. *Proceedings of Geotechnical Engineering for Transportation Projects*, Los Angeles, CA.

Boulanger, R.W., Wilson, D.W., Kutter, B.L., DeJong, J.T., and Bronner, C.E. NHERI centrifuge facility: large-scale centrifuge modeling in geotechnical research. *Frontiers in the Built Environment*, 6(121), 1-17.

Boulon, M., & Foray, P. (1986). Physical and Numerical Simulation of Lateral Shaft Friction Along Offshore Piles in Sand. *Proceedings, Third International Conference on Numerical Methods in Offshore Piling*, 127-147, Nantes, France.

Burrall, M., DeJong, J.T., Martinez, A, & Wilson, D.X. (2020) Vertical Pullout Tests of Orchard Trees for Bio-inspired Engineering of Anchorage and Foundation Systems. *Bioinspiration and Biomimetics*, 16(1).

Carey, T. J., Stone, N., & Kutter, B. L. (2019). Grain Size Analysis and Maximum and Minimum Dry Density Testing of Ottawa F-65 Sand for LEAP-UCD-2017. *Model Tests and Numerical Simulations of Liquefaction and Lateral Spreading, LEAP-UCD-2017*, Davis, CA.

Chen, Y. J., & Kulhawy, F. H. (1994). Case history evaluation of the behavior of drilled shafts under axial and lateral loading. *EPRI TR-104601*, Palo Alto, CA.

Chen, Y., Khosravi, A., Martinez, A., and DeJong, J.T. Modeling the self-penetration process of a bio-inspired probe in granular soils. In press for publication in *Bioinspiration and Biomimetics*.

Darby, K.M., Boulanger, R.W., DeJong, J.T., and Bronner, J.D. (2019a). Progressive changes in liquefaction and cone penetration resistance across multiple shaking events in centrifuge tests. *Journal of Geotechnical and Geoenvironmental Engineering*, 145(3).

DeJong, J. T., Burrall, M., Wilson, D. W., & Frost, J. D. (2017). A bio-inspired perspective for geotechnical engineering innovation. *Proceedings of Geofrontiers*, 862-870, Orlando, FL.

Fellenius, B. H. (1972). Downdrag on long piles in clay due to negative skin friction. *Canadian Geotechnical Journal*, 9(4), 323-337.

FHWA (2016) Design and Construction of Driven Pile Foundations. *National Highway Institute, Geotechnical Engineering Circular No. 12 – Volume I,* Washington.

Fioravante, V., Ghionna, V. N., Jamiolkowski, M., & Sarri, H. (1999). Shaft friction moeling of non-displacement piles in sand. *Proceedings of analysis design, construction and testing of deep foundations*, 1-24, Austin, TX.

Fioravante, V. (2002). On the shaft friction modelling of non-displacement piles in sand. *Soils and Foundations*, 42(2), 23–33. doi:10.3208/sandf.42.2_23

Garnier, J., Gaudin, C., Springman, S. M., Culligan, P. J., Goodings, D., Konig, D., Kutter, B.L., Phillips, R., Randolph, M. F., & Thorel, L. (2007). Catalogue of scaling laws and similitude questions in geotechnical centrifuge modelling. *International Journal of Physical Modelling in Geotechnics*, 7(3). doi:10.1680/ijpmg.2007.070301

Houlsby, G. T., & Byrne, B. W. (2005). Design procedures for installation of suction caissons in sand. *Geotechnical Engineering*, 158(GE3). doi:10.1680/geng.2005.158.3.135

Huang, S., & Tao, J. (2020). Modeling Clam-inspired Burrowing in Dry Sand using Cavity Expansion Theory and DEM. *Acta Geotechica*. doi:10.1007/s11440-020-00918-8

Jardine, R. J., Lehane, B. M., & Everton, S. J. (1992). Friction coefficients for piles in sands and silts. *Proceedings of Offshore Site Investigation and Foundation Behavior*, 661-677. London, UK.

Kutter, B.L. (1992). Dynamic centrifuge modeling of geotechnical structures. *Transportation Research Record* 1336, TRB, National Research Council, 24-30.

Kulic, I. M., Mani, M., Mohrbach, H., Thaokar, R., & Mahadevan, L. (2009). Botanical Ratchets. *Proceedings*

of the Royal Society B., 276(1665), 2243-2247. doi:10.1098/rspb.2008.1685

Lehane, B. M., Jardine, R. J., Bond, A. J., & Frank, R. (1993). Mechanisms of shaft friction in sand from instrumented pile tests. *Journal of Geotechnical Engineering*, 119(1), 19–35. doi:10.1061/(ASCE)0733-9410(1993)119:1(19)

Lehane, B. M., Schneider, J. A., & Xu, X. (2005). A review of design methods for offshore driven piles in siliceous sand. *University of Western Australia, GEO 05358*, Perth, Australia.

Loganathan, N., Poulos, H. G., & Stewart, D. P. (2000). Centrifuge model testing of tunnel-induced ground and pile deformations. *Géotechnique*, 50(3), 283-294. doi:10.1680/geot.2000.50.3.283

Martinez, A., Frost, J. D., & Hebeler, G. J. (2015). Experimental study of shear zones formed at sand/steel interfaces in axial and torsional axisymmetric tests. *Geotechnical Testing Journal*, 38(4), 409-426. doi:10.1520/GTJ20140266

Martinez, A., & Frost, J. D. (2017). The influence of surface roughness form on the strength of sand-structure interfaces. *Geotechnique Letters*, 7(1), 104-111. doi:10.1680/jgele.16.00169

Martinez, A., Palumbo, S., & Todd, B. D. (2019). Bio-Inspiration for anisotropic load transfer at soil-structure interfaces. *Journal of Geotechnical and Geoenvironmental Engineering*, 145(10). doi:10.1061/(ASCE)GT.1943-5606.0002138

Martinez, A., DeJong, J. T., Jaeger, R., & Khosravi, A. (2020). Evaluation of self-penetration potential of a bio-inspired site characterization probe by cavity expansion analysis. *Canadian Geotechnical Journal*, 57(5). doi:10.1139/cgj-2018-0864

Martinez, A., DeJong, J., Akin, I., Aleali, A., Arson, C., Atkinson, J., Bandini, P., Baser, T., Borela, R., Boulanger, R., Burrall, M., Chen, Y., Collins, C., Cortes, D., Dai, S., DeJong, T., Del Dottore, E., Dorgan, K., Fragaszy, R., Frost, D., Full, R., Ghayoomi, M., Goldman, D., Gravish, N., Guzman, I. L., Hambleton, J., Hawkes, E., Helms, M., Hu, D. L., Huang, L., Huang, S., Hunt, C., Irschick, D., Lin, H., Lingwall, B., Marr, W. A., Mazzolai, B., McInroe, B., Murthy, T., O'Hara, K., Porter, M., Sadek, S., Sanchez, M., Santamarina, C., Shao, L., Sharp, J., Stuart, H., Stutz, H. H., Summers, A. P., Tao, J., Tolley, M., Treers, L., Turnbull, K., Valdes, R., van Passen, L., Viggiani, G., Wilson, D., Wu, W., Yu, X., & Zheng, J. (2021). Bio-inspired Geotechnical Engineering: Principles, Current Work, Opportunities and Challenges. In press for publication in *Géotechnique*. doi: 10.1680/jgeot.20.P.170

Marvi, H., & Hu, D. L. (2012). Friction enhancement in concertina locomotion of snakes. *Journal of the Royal Society Interface*, 9(76), 3067–3080. doi:10.1098/rsif.2012.0132

Mason, H. B., Trombetta, N. W., Chen, Z., Bray, J. D., Hutchinson, T. C., & Kutter, B. L. (2013). Seismic soil-foundation-structure interaction observed in geotechnical centrifuge experiments. *Soil Dynamics and Earthquake Engineering*, 48(May), 162-174. doi:10.1016/j.soildyn.2013.01.014

De Nicola, A., & Randolph, M. F. (1999). Centrifuge modeling of pipe piles in sand under axial loads. *Géotechnique,* 49(3), 295-318. doi:10.1680/geot.1999.49.3.295

Noel, A. C., & Hu, D. L. (2018). Cats use hollow papillae to wick saliva into fur. *Proceedings of the National Academy of Sciences*, 115(49), 12377-12382. doi:10.1073/pnas.1809544115

Nova Roessig, L., & Sitar, N. (2006). Centrifuge model studies on the seismic response of reinforced soil slopes. *Journal of Geotechnical and Geoenvironmental Engineering*, 132(3), 388-400. doi:10.1061/(ASCE)1090-0241(2006)132:3(388)

O'Hara, K. B., & Martinez, A. (2020). Monotonic and Cyclic Frictional Anisotropy in Snakeskin-Inspired Surfaces and Piles. Accepted for Publication in the *Journal of Geotechnical and Geoenvironmental Engineering*, 146(11). doi:10.1061/(ASCE)GT.1943-5606.0002368

Palumbo, S. (2018). Anisotropic interface shear behavior of granular soil and surfaces biologically-inspired by snakeskin. M.S. thesis, Department of Civil and Environmental Engineering, University of California, Davis.

Salgado, R. (2008). *The engineering of foundations*. New York, NY: McGraw-Hill.

Sturm, A., Shepard, G., DeJong, J., & Wilson, D. W. (2018). A Centrifuge Study on the Effects of Soil Gradation on Liquefaction Potential and Dynamic Response. *Proceedings of ASDSO Conference*, Seattle, WA, 2018.

Stutz, H.H. and Martinez, A. (2021). Directionally-dependent strength and dilatancy behavior of soil–structure interfaces. In press for *Acta Geotechnica*.

Tehrani, F. S., Han, F., Salgado, R., Prezzi, M., Tovar, R. D., & Castro, A. G. (2016). Effect of surface roughness on the shaft resistance of non-displacement piles embedded in sand. *Géotechnique*, 66(5). doi: 10.1680/jgeot.15.P.007

Tsuha, C. H. C., Foray, P. Y., Jardine, R. J., Yang, Z. X., Silva, M., & Rimoy, S. (2012). Behaviour of displacement piles in sand under cyclic axial loading. *Soils and Foundations*, 52(3), 393-410. doi:10.1016/j.sandf.2012.05.002

Wei, J., & El Naggar, M. H. (1998). Experimental study of axial behavior of tapered piles. *Canadian Geotechnical Journal*, 35(4), 641-654. doi:10.1139/t98-033

White, D. J., & Lehane, B. M. (2004). Friction fatigue on displacement piles in sand. *Géotechnique*, 54(10), 645-658. doi:10.1680/geot.2004.54.10.645